Effect of Surface Modification on Magnetization of Iron Oxide Nanoparticle Colloids

ARTICLE *in* LANGMUIR · AUGUST 2012

Impact Factor: 4.46 · DOI: 10.1021/la3022479 · Source: PubMed

6 AUTHORS, INCLUDING:

Deniz Rende
Rensselaer Polytechnic Institute
39 PUBLICATIONS **106** CITATIONS
SEE PROFILE

Seyda Bucak
Yeditepe University
36 PUBLICATIONS **575** CITATIONS
SEE PROFILE

Rahmi Ozisik
Rensselaer Polytechnic Institute
103 PUBLICATIONS **1,864** CITATIONS
SEE PROFILE

Diana-Andra Borca-Tasciuc
Rensselaer Polytechnic Institute
67 PUBLICATIONS **533** CITATIONS
SEE PROFILE

Langmuir

Article

pubs.acs.org/Langmuir

Effect of Surface Modification on Magnetization of Iron Oxide Nanoparticle Colloids

Yuan Yuan,[†] Deniz Rende,[‡,∥] Cem Levent Altan,[∥,⊥] Seyda Bucak,[∥] Rahmi Ozisik,[‡,§] and Diana-Andra Borca-Tasciuc*,[†]

[†]Mechanical, Aerospace and Nuclear Engineering Department, [‡]Rensselaer Nanotechnology Center, and [§]Department of Materials Science and Engineering, Rensselaer Polytechnic Institute, Troy, New York 12180, United States

[∥]Department of Chemical Engineering, Yeditepe University, Istanbul, 34755, Turkey

[⊥]Laboratory of Materials and Interface Chemistry, Eindhoven University of Technology, P.O. Box 513, 5600 MB Eindhoven, The Netherlands

Supporting Information

ABSTRACT: Magnetic iron oxide nanoparticles have numerous applications in the biomedical field, some more mature, such as contrast agents in magnetic resonance imaging (MRI), and some emerging, such as heating agents in hyperthermia for cancer therapy. In all of these applications, the magnetic particles are coated with surfactants and polymers to enhance biocompatibility, prevent agglomeration, and add functionality. However, the coatings may interact with the surface atoms of the magnetic core and form a magnetically disordered layer, reducing the total amount of the magnetic phase, which is the key parameter in many applications. In the current study, amine and carboxyl functionalized and bare iron oxide nanoparticles, all suspended in water, were purchased and characterized. The presence of the coatings in commercial samples was verified with X-ray photoelectron spectroscopy (XPS). The class of iron oxide (magnetite) was verified via Raman spectroscopy and X-ray diffraction. In addition to these, in-house prepared iron oxide nanoparticles coated with oleic acid and suspended in heptane and hexane were also investigated. The saturation magnetization obtained from vibrating sample magnetometry (VSM) measurements was used to determine the effective concentration of magnetic phase in all samples. The Tiron chelation test was then utilized to check the real concentration of the iron oxide in the suspension. The difference between the concentration results from VSM and the Tiron test confirmed the reduction of magnetic phase of magnetic core in the presence of coatings and different suspension media. For the biocompatible coatings, the largest reduction was experienced by amine particles, where the ratio of the effective weight of magnetic phase reported to the real weight was 0.5. Carboxyl-coated samples experienced smaller reduction with a ratio of 0.64. Uncoated sample also exhibits a reduction with a ratio of 0.6. Oleic acid covered samples show a solvent-depended reduction with a ratio of 0.5 in heptane and 0.4 in hexane. The corresponding effective thickness of the nonmagnetic layer between magnetic core and surface coating was calculated by fitting experimentally measured magnetization to the modified Langevin equation.

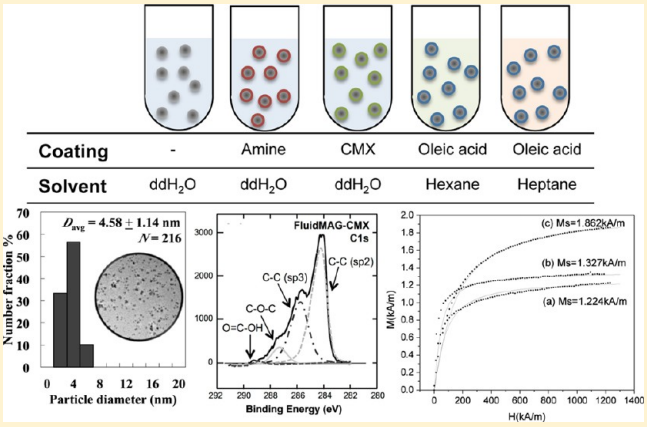

1. INTRODUCTION

Iron oxide magnetic nanoparticles are of great interest because of their unique physical and chemical properties due to their extremely small size and large specific surface area.[1] They have been extensively studied in recent years for their promising applications in the biomedical field, such as drug delivery,[2−4] immunoassay analyzer,[5−7] magnetic resonance imaging (MRI),[8−11] and cancer hyperthermia.[12−14] In all of these applications, the magnetic particles are coated with surfactants and polymers to enhance biocompatibility, provide functionality (i.e., via functional groups that can target specific biomolecules), and prevent agglomeration. However, the coating may interact with the surface atoms of the magnetic core to form a nonmagnetic layer, reducing its effective size and the total amount of magnetic phase. The effective size and especially the concentration of the magnetic phase are important factors in many biomedical applications. For instance, in magnetic nanoparticle-mediated cancer hyperthermia, these two parameters control the heat generation rate, which in turn determine the efficacy of the treatment.[15]

Received: June 1, 2012
Revised: August 9, 2012
Published: August 14, 2012

Specifically, the power dissipated by superparamagnetic nanoparticles is linear with equilibrium susceptibility, which is proportional to $\varphi \cdot V$ product, where φ is the volumetric concentration and V is the volume of the magnetic core.[16] In MRI, the magnetic nanoparticles act as contrast agents that increase the relaxation rate of the nuclei of interest. The relaxivity, which defines the ability of a fixed concentration of the contrast agent to increase the relaxation rate, is sensitive to the particle size and linearly depends on the concentration of the magnetic core.[17] To optimize the properties of the magnetic nanoparticles for these applications, it is essential to understand how coatings modify the effective size of the magnetic core. Only a few studies have been reported on the reduction of the magnetic phase in coated nanoparticle systems, and none have focused on biocompatible coatings.[18−20] All indicated that the properties of magnetic nanoparticles change after chemical surface modification. One of the earliest works was reported by Kaiser et al.,[18] who showed that the saturation magnetization of magnetite nanoparticles coated with oleic acid depends on the solvent. Later, Chantrell et al.[19] extended the studies to more solvents and different particle sizes, all dispersed with oleic acid. They showed that the saturation magnetization of the ferrofluid was less than the product of saturation magnetization of the bulk material and volume fraction of nanoparticles. The decrease was attributed to the surface chemical interaction between the stabilizing surfactant and the magnetic core. More recently, Vestal and Zhang[20] also showed that the coercivity and saturation magnetization of manganese ferrite nanoparticle change after surface modification with para-substituted benzoic acid ligands and substituted benzene ligands.

As mentioned above, none of these studies were carried out for coatings relevant to biomedical applications. In the current work, commercially available magnetic nanoparticles suspended in water and having different biocompatible coatings or no coating were investigated. For comparison, oleic acid-coated iron oxide nanoparticles suspended in hexane and heptane were also studied. All particles were characterized by transmission electron microscopy (TEM) to determine their physical size. X-ray diffraction (XRD) and Raman spectroscopy were performed to confirm the class of iron oxide. X-ray photoelectron spectroscopy (XPS) was utilized to verify the coatings of the commercial samples. The saturation magnetization obtained from vibrating sample magnetometry (VSM) measurements was used to determine the apparent concentration of magnetic phase by normalization to saturation value of bulk iron oxide. The results were then compared against real concentrations determined from Tiron chelation test (which is a direct measurement of iron content) to determine the reduction in the magnetic phase for each type of coating and solvent used. The thickness of nonmagnetic layer between magnetic core and surface coating was calculated by fitting the experimental magnetization to the modified Langevin equation.

2. MATERIALS AND METHODS

2.1. Materials. Commercially available nanoparticle suspensions, FluidMAG-Amine, FluidMAG-UC/A, and FluidMAG-CMX, in water, were purchased from Chemicell.[21] The nanoparticles in FluidMAG-UC/A have no functional group (are uncoated), although they do have a positive surface charge. The aminosilane-coated nanoparticles in FluidMAG-Amine have an amine ($-NH_2$) functional group, while the carboxymethyl-dextran-coated nanoparticles in FluidMAG-CMX are terminated in the carboxyl ($-COOH$) group. The chemical structure of the coating is provided in more detail on the manufacturer's Web site.[21] These functional coatings were selected for their wide range of applications in bioconjugation techniques; they are often linked to cell-targeting agents.[22,23]

Aside from commercially available ferrofluids, oleic acid-coated iron oxide nanoparticles were synthesized in-house and suspended in hexane (MAG/OA-HEX) and heptane (MAG/OA-HEP). The method used in the synthesis of the magnetic nanoparticles in oil is an adaptation of a previously reported protocol, which is presented in the Supporting Information.[24] Oleic acid, which is a hydrophobic surface ligand, covalently binds to surface hydroxyl molecules via its carboxyl end, leaving the hydrophobic tail free,[25] which facilitates suspension in polar solvents.

2.2. Characterization of Magnetic Nanoparticles. The morphology of the nanoparticles in all samples was first investigated using a JEOL 2011 transmission electron microscope operating at 200 kV. The TEM samples were prepared by diluting the commercial samples with water (100× v/v) and the oleic acid-coated sample by either heptane or hexane (100× v/v), then placing a droplet of the diluted suspension on a carbon-coated copper grid. The class of iron oxide as well as the crystallinity of the particles were first checked by X-ray diffraction on an X'Pert PRO machine from PANalytical. The XRD samples were prepared by placing a droplet of a sample on a silicon-based sample holder and drying at 70 °C. Data were collected with an X'Pert Data Collector, taking measurements of 2θ from 20° to 70° at 100 steps.

Raman microscopy was performed to complement the X-ray diffraction results. Confocal Raman microscopy (WITec 300R) equipped with a 532 nm green light laser and CCD camera was used to characterize the samples by single spectrum acquisition with 1 s integration time and 30 accumulations. An integrated confocal microscope, with a 10× objective, was used to focus the laser. The laser power was in the range of 0.04−0.2mW and calibrated with a Newport Optical Power/Energy Meter before each use. The WITech project software package was used for data analysis. For the Raman measurements, a 20 uL drop of ferrofluid was deposited on a microscope glass cover slide and dried at 40 °C in the dark for 24 h. The dehydrated sample was then placed on the automated stage. The raw data collected for three spectra were then averaged to obtain the final representation.

The existence of surface coatings on commercial samples FluidMAG-UC/A, FluidMAG-Amine, and FluidMAG-CMX was verified with X-ray photoelectron spectroscopy. XPS was carried out on a PHI VersaProbe 5000 instrument having monochromatic 100 μm beam of Al Kα radiation as X-ray source. Wide scan surveys and specific regions (for example, C1s, N1s) were measured with a step size of 0.2 eV. X-ray spectra were recorded with a 23.5 or 58.7 eV pass energy with an average of 25 scans for specific regions. The charge neutralizer was kept on the off-position, and calibration of binding energy was performed using C1s at 284.8 eV as a reference. Further data processing was performed with Physical Electronics MultiPAK v9.0 software. Following the subtraction of the background, specific spectra were fitted with 60% Gaussian/40% Lorentzian peaks, taking the minimum number of peaks consistent with the best fit.

The magnetization was measured via a vibrating sample magnetometer (Lake Shore, Inc.). The measurement was performed at room temperature using approximately 60 μL volume of sample. During VSM measurement, sample magnetization was recorded as a function of the applied magnetic field. Field strength was varied in the range of ±1500 kA/m at an operating frequency of 80 Hz.

2.3. Colorimetric Determination of Concentration with Tiron Chelation Test. The Tiron chelation test was used to determine the iron concentration, which can then be converted to the real concentration of magnetite. Tiron (4,5-dihydroxy-1,3-benzenedisulfonic acid disodium salt) chelates with Fe^{3+} and Fe^{2+} ions in a ratio of three Tiron molecules to each iron molecule and exhibits a consistent and strong absorbance at 480 nm for iron solutions with a pH greater than 9.5.[26] To liberate the iron content of the magnetite, concentrated hydrochloric acid solution was added to the magnetic fluid. The hydrochloric acid also aids removal of the coating around the magnetite. The absorbance of the diluted sample was then

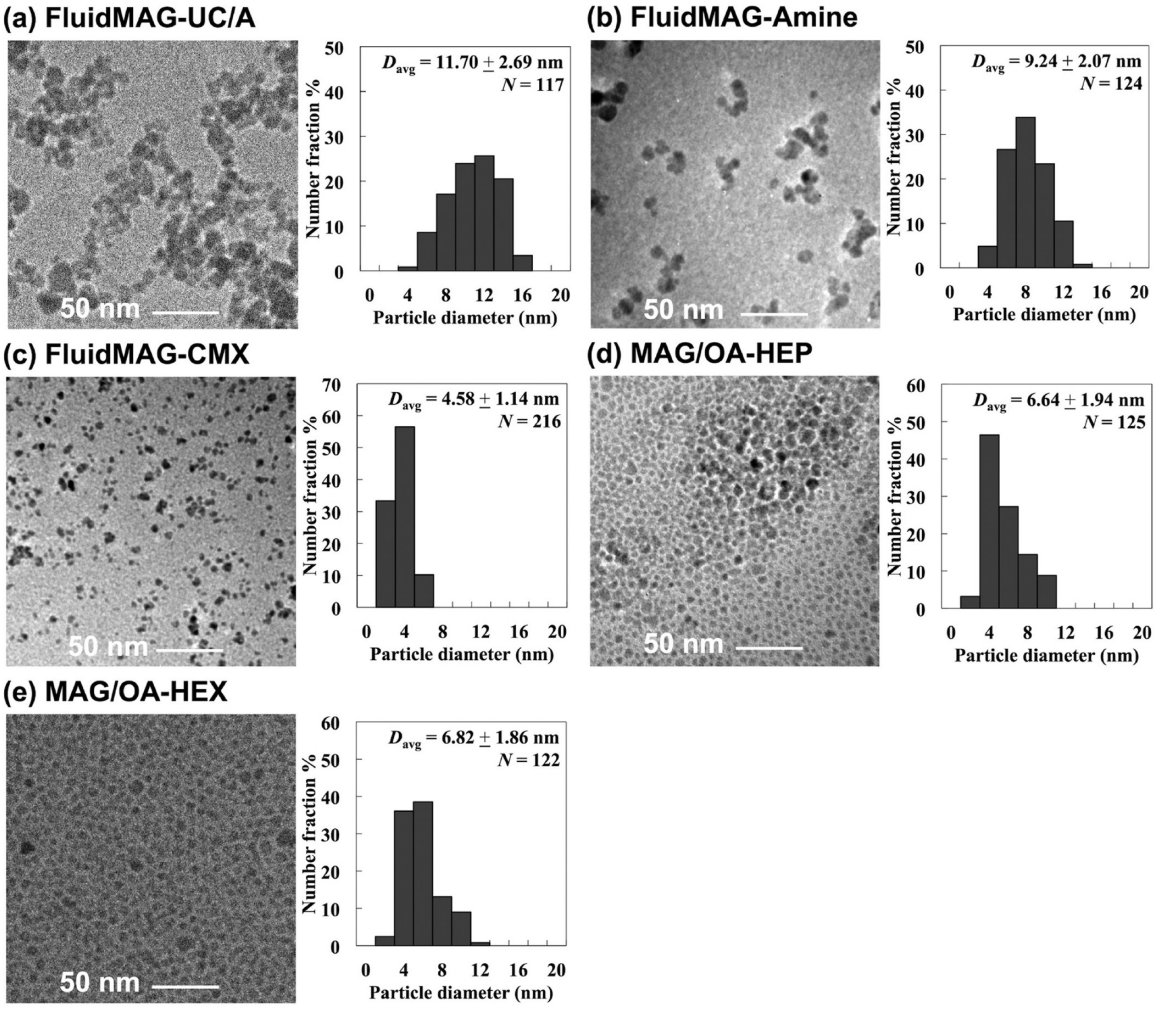

Figure 1. TEM images and the corresponding particle size histograms of (a) FluidMAG-UC/A, (b) FluidMAG-Amine, (c) FluidMAG-CMX, (d) MAG/OA-HEP, and (e) MAG/OA-HEX.

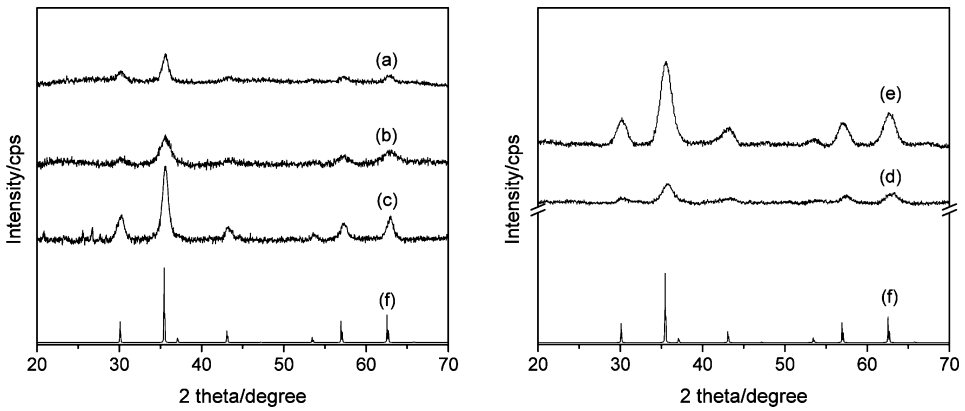

Figure 2. X-ray powder diffraction patterns of (a) FluidMAG-UC/A, (b) FluidMAG-CMX, (c) FluidMAG-Amine, (d) MAG/OA-HEP, (e) MAG/OA-HEX, and (f) simulated powder diffraction data for magnetite.[27]

measured with a spectrophotometer and converted to concentration of the magnetite in the sample solution as explained in the Supporting Information.

3. RESULTS AND DISCUSSION

3.1. Characterization of Magnetic Nanoparticles. The TEM images as well as size distributions of FluidMAG-UC/A, FluidMAG-Amine, FluidMAG-CMX, and oleic acid-coated iron oxide nanoparticles suspended in heptane and hexane are shown in Figure 1a–e, respectively.

The number of nanoparticles subjected to analysis, the average particle diameter, and the corresponding standard deviation are summarized in each corresponding histogram. The particle size of uncoated FluidMAG-UC/A (Figure 1a) was measured as 11.7 ± 2.69 nm. The high standard deviation

dx.doi.org/10.1021/la3022479 | *Langmuir* 2012, 28, 13051–13059

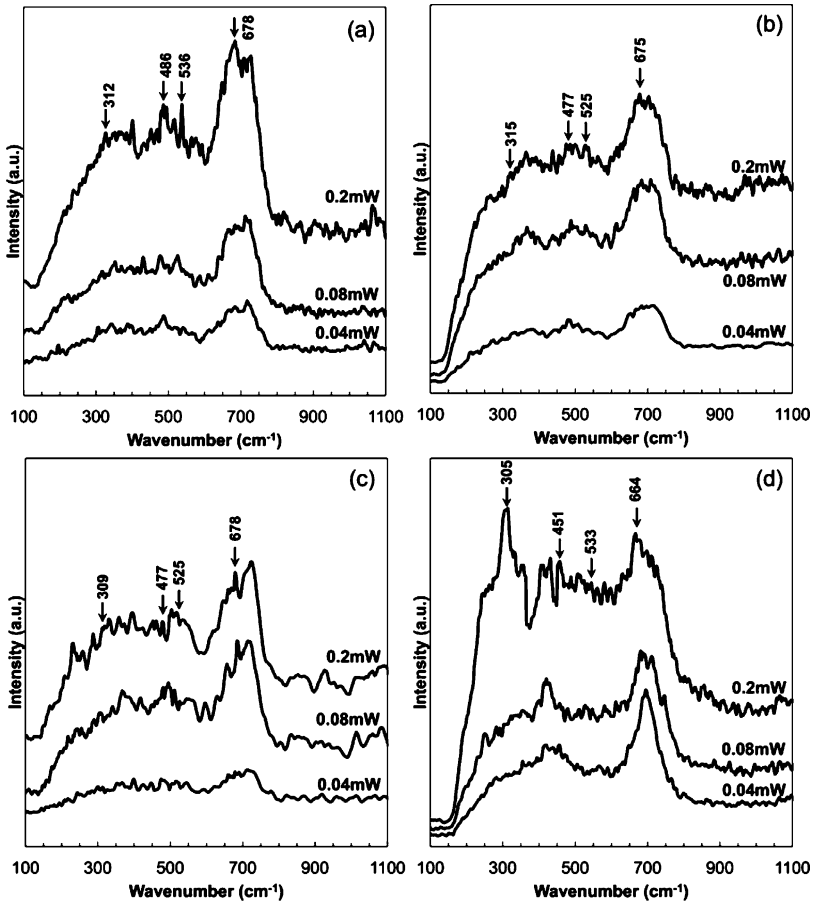

Figure 3. Intensity as a function of wavelength from confocal Raman measurements of (a) FluidMAG-UC/A, (b) FluidMAG-Amine, (c) FluidMAG-CMX, and (d) MAG-OA.

Table 1. Summary of the Raman Frequencies (cm^{-1}) of the Samples

mode	FluidMAG-UC/A	FluidMAG-Amine	FluidMAG-CMX	MAG-OA	Chourpa, 2005[32]	Shebanova, 2003[31]
A_{1g}	678	675	678	664	662	668
$T_{2g}(2)$	536	525	525	533	528	538
$T_{2g}(3)$	486	477	477	451	456−508	450−490
E_g	312	315	309	305	303	306

in this measurement indicates a wide size distribution. The particle size of aminosilane-coated (FluidMAG-Amine, Figure 1b) particles was determined as 9.24 ± 2.09 nm. The particle size of carboxymethyl-dextran-coated magnetic nanoparticles (FluidMAG-CMX, Figure 1c) was 4.58 ± 1.14 nm. The size of these particles was observed to be quite uniform as compared to uncoated magnetic nanoparticles. In addition, nanoparticle clusters were obvious in TEM images of FluidMAG-Amine and FluidMAG-UC/A, while nanoparticles appeared to be better dispersed in FluidMAG-CMX. The in-house synthesized oleic acid-coated magnetic nanoparticles suspended in hexane and heptane had identical sizes and similar standard deviation at 6.64 ± 1.94 nm and 6.82 ± 1.86 nm, respectively (Figure 1d and e). This was expected because both suspensions were prepared using particles synthesized in the same process.

X-ray diffraction was first employed to assess the type of iron oxide of all particles. The XRD spectra match the standard (Fe_3O_4) crystal structure data, as shown in Figure 2.

However, because X-ray diffraction patterns of magnetite and maghemite are the same, Raman spectroscopy was also carried out to verify the magnetite state. The results are presented in Figure 3. To prevent the laser-induced transformation into hematite,[28−30] the laser power utilized was less than 0.2 mW. The intensity peaks are compared to those reported for confocal Raman microspectroscopy on ferrite-based nanoparticles;[31,32] all main peaks are summarized in Table 1. As seen from Table 1 and Figure 3, all samples have a distinguishable intense peak around 670 cm^{-1} (A_{1g} mode), which is accepted as the signature peak position of bulk magnetite.[28,30−34] Three other theoretical phonon frequencies of magnetite exhibit peaks at 303−306 (E_g), 450−510 ($T_{2g}(3)$), and 528−538 ($T_{2g}(2)$) cm^{-1}.[31,32] The uncoated iron oxide sample (FluidMAG-UC/A), along with an intense peak at 678 cm^{-1}, has signals at 312, 486, and 536 cm^{-1}, which is in good agreement with previous studies.[31] The wide range of peak around 700−720 cm^{-1} is attributed to maghemite,[31,32,34,35] a possible indication of oxidation during sample preparation or analysis (drying at 40 °C).[36] Amine-coated iron oxide nanoparticles (FluidMAG-Amine) have an intense peak at 675 cm^{-1} with other peak positions at 315, 477, and 525 cm^{-1}. The carboxy methyl dextran-coated nanoparticles (FluidMAG-CMX) have also a distinct intense peak at 678 cm^{-1}, accompanied by the maxima

dx.doi.org/10.1021/la3022479 | Langmuir 2012, 28, 13051−13059

at 309, 477, and 525 cm^{-1}. The shoulders at 277 and 326 cm^{-1} provide additional evidence that these samples are magnetite.[32] The in-house synthesized oleic acid-coated magnetic nanoparticles (MAG-OA) also have an intense peak at 664 cm^{-1}, with peaks at 305, 451, and 533 cm^{-1}, suggesting that the synthesis protocol followed in this study produces magnetite nanoparticles.

The presence of the coatings in commercial samples was verified with XPS. Wide range scans for FluidMAG-UC/A, FluidMAG-Amine, FluidMAG-CMX, and the carbon tape used to mount the samples are shown in Figure 4. The regions

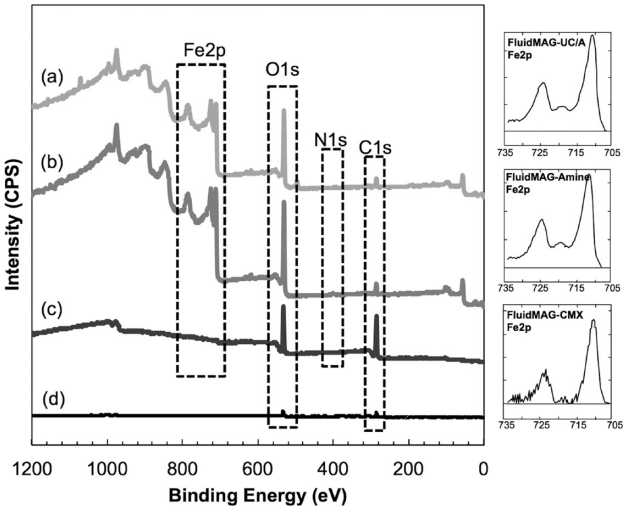

Figure 4. XPS spectra in the Fe2p, O1s, N1s, C1s, and Si2p regions for (a) FluidMAG-UC/A, (b) FluidMAG-Amine, (c) FluidMAG-CMX, and (d) carbon tape. The insets represent high-resolution Fe2p regions for the samples.

scanned with high resolution and used for surface analysis are marked in this figure. The inset figures show Fe $2p_{3/2}$ and $2p_{1/2}$ peaks for FluidMAG-UC/A, FluidMAG-Amine, and FluidMAG-CMX samples at 711.0 and 724.6 eV binding energies, respectively. They are all in good agreement with the literature.[37−41] The low intensity values of Fe2p peaks in FluidMAG-CMX suggest that a dense carboxymethyl dextran coating is present on the surface, preventing the penetration of X-rays to the magnetic core. The hydroxyl groups on the surface of uncoated iron oxide nanoparticles (FluidMAG-UC/A) and amine-coated nanoparticles (FluidMAG-Amine) exhibit an O1s peak at 530.2 eV.[40] FluidMAG-CMX has a O1s peak at 532.4 eV, which is characteristic of carboxymethyl dextran coating.[42]

More details of the coating composition can be seen in Figure 5. FluidMAG-UC/A and FluidMAG-Amine dried out as fine powder, and they had to be supported with carbon tape during measurements. The carbon tape produced two C1s peaks at 285.0 and 288.9 eV (Figure 5c), which were also observable in the experimental data of both type of particles (Figure 5a and b).

The FluidMAG-Amine contains an aminosilane group where the amino group is exposed to the free surface of the particle.[21] The existence of this group is observed in this sample only with two peaks at 399.9 and 401.0 eV, which corresponds to $-NH_2$ groups (Figure 5d).[43]

It should be noted that FluidMAG-CMX, which dried out in the form of flakes, could be measured without the need of a supporting carbon tape. Hence, in its high-resolution scan, all signal comes from the sample itself, which appears to have a carbon-rich surface coating with a broad C1s spectrum (Figure 5e). For instance, the peaks at 284.41 and 286.9 eV correspond to the C−C bond in sp^2 and sp^3 structure, respectively, while the peaks at 287.4 and 288.9 eV correspond to C−O−C bond and carboxyl group (−COOH), respectively, in the carboxyl methyl dextran structure.[44] These results confirmed the existence of the coatings as reported by the manufacturer.

3.2. Magnetic Phase Reduction. In Tiron chelation test, the absorbance of the samples was measured at 480 nm. On the basis of the adsorption wavelength, the mass concentration was calculated and is shown in Table 2.

The room temperature magnetization curves for all samples are shown in Figure 6. The saturation magnetization of the samples obtained from VSM can be used to estimate the volumetric concentration of the magnetic phase, φ,[45] as follows:

$$\varphi = \frac{M_s}{M_b} \tag{1}$$

where M_s and M_b are saturation magnetization of the magnetic fluid and bulk iron oxide (446 kA/m[19]), respectively. On the basis of the volumetric concentration, the mass concentration of the nanoparticles in solution was determined from: $C_M = \varphi \cdot \rho_p$, where ρ_p is the mass density of magnetite (5.18 g/mL).[16]

Table 2 shows the mass concentration as calculated from the magnetization curves and from the Tiron test together with their ratio. This ratio represents the proportion of magnetic phase to the entire magnetite mass present in solution. As expected, the magnetization measurements indicate a smaller amount of iron oxide due to the reduction in the magnetic phase resulting from surface modifications.[18,46]

To extract information about the effective radius of the magnetic domain and the thickness of the nonmagnetic layer, the experimental magnetization is fitted by the modified Langevin model.[18] For polydispersed suspensions, the magnetization of the ferrofluid of volume V_o with n_i particles of magnetic core size v_i can be calculated by taking size distribution into account as:

$$\frac{M}{M_b} = \sum_{i=1}^{\infty} \left\{ \coth\left(\frac{v_i M_b H}{4\pi kT}\right) - \frac{4\pi kT}{v_i M_b H} \right\} n_i v_i / V_o \tag{2}$$

where k is the Boltzmann constant, T is the absolute temperature, H is the applied field, and M_b is the bulk magnetization of the material.

The volume concentration, φ_0, of the total amount of magnetite is:

$$\varphi_0 = \left(\sum_{i=1}^{\infty} n_i V_i \right) / V_o \tag{3}$$

where $V_i = (\pi/6) \cdot D_i^3$ is the total volume of the particle, including the nonmagnetic iron oxide surface layer. Denoting with a_0 the thickness of the nonmagnetic layer formed at the interface due to the presence of the coating, the effective volume of iron oxide magnetic core can be expressed as:

$$v_i = \frac{\pi}{6} \cdot (D_i - 2a_0)^3 \tag{4}$$

Substituting eqs 3 and 4 into eq 2, the final expression for saturation magnetization as a function of material properties and applied field is then:

dx.doi.org/10.1021/la3022479 | Langmuir 2012, 28, 13051−13059

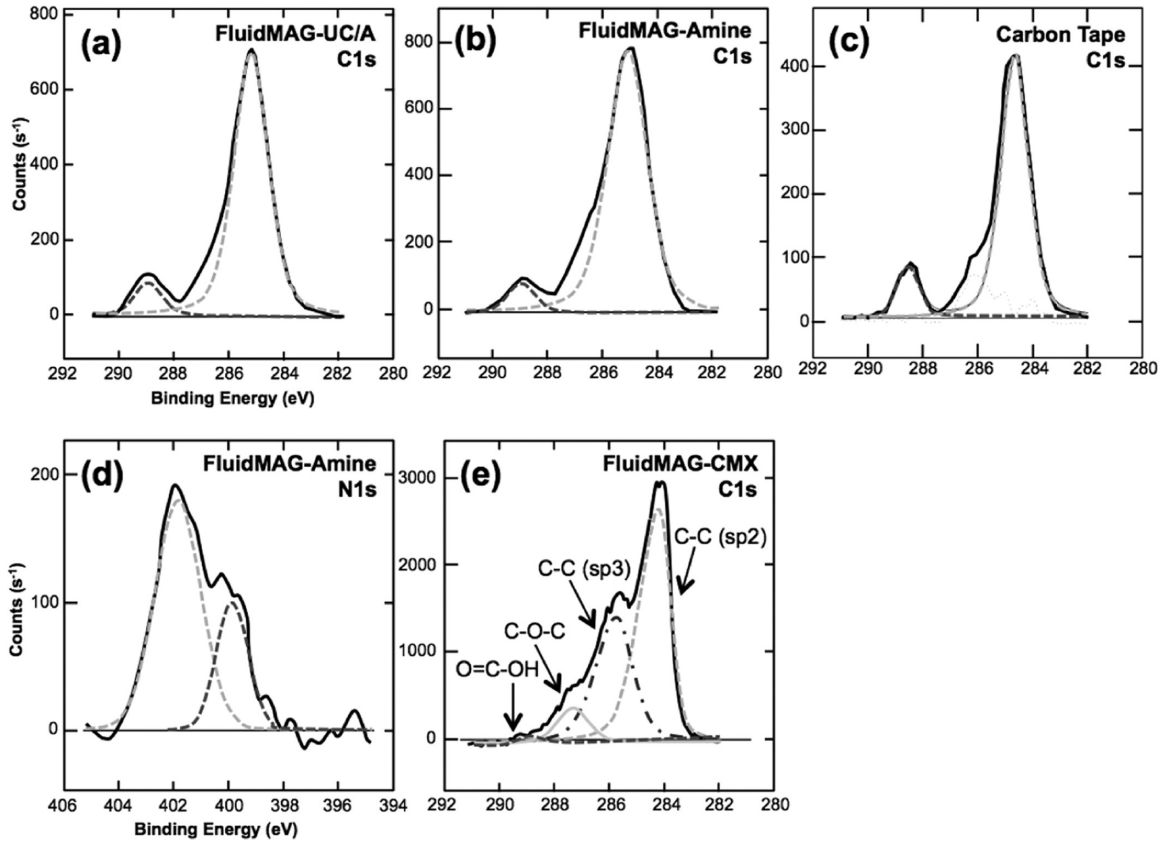

Figure 5. High-resolution spectra of C1s regions of (a) FluidMAG-UC/A, (b) FluidMAG-Amine, (c) carbon tape, (d) N1s region of FluidMAG-Amine, and (e) C1s region of FluidMAG-CMX.

Table 2. Mass Concentration of Magnetic Phase As Calculated from Magnetization Curves (C_M) and from Tiron Chelation Test (C_T)[a]

sample	Tiron test C_T (mg/mL)	magnetization test C_M (mg/mL)	magnetization/ Tiron (C_M/ C_T)	a_0 (nm)
FluidMAG-UC/A	23.6	14.2	0.602	1.06 ± 0.34
FluidMAG-Amine	30.9	15.4	0.498	1.51 ± 0.51
FluidMAG-CMX	33.8	21.6	0.639	0.54 ± 0.22
MAG/OA-HEP	28.2	14.9	0.528	0.58 ± 0.07
MAG/OA-HEX	14.9	5.9	0.396	0.97 ± 0.12

[a]Their ratio is also shown together with the predicted thickness of the nonmagnetic surface layer (a_0).

$$\frac{M}{\varphi_0 M_b} = \sum_{i=1}^{\infty} \left\{ \coth\left(\frac{(D_i - 2a_0)^3 M_b H}{24kT}\right) - \frac{24kT}{(D_i - 2a_0)^3 M_b H} \right\} n_i (D_i - 2a_0)^3 / \sum_{i=1}^{\infty} n_i D_i^3 \quad (5)$$

The above equation was fitted against experimental magnetization as a function of the applied field. For this process, the numbers of n_i particles and the corresponding diameter D_i were obtained from the histograms in Figure 1. The volume concentration of total magnetite φ_0 was determined as $\varphi_0 = C_T/\rho_p$, where C_T is the mass concentration from the Tiron chelation test.

The optimum fitting together with their corresponding experimental magnetization curves are shown in Figure 6. The effective thickness of the nonmagnetic iron oxide surface layer was determined from the fitting as follow. On the basis of the size distribution of nanoparticles from TEM images, three optimal a_0 values for each magnetization curve were obtained. Their average values and standard errors were then calculated, and the results are shown in Table 2.

Of special interest are particles in FluidMAG-UC/A, which have no coating, yet they still show a reduction in magnetization with an effective nonmagnetic layer of approximately 1 nm. Most likely this comes from the positive surface charge, which may modify the electron states causing some disorder at the surface. In turn, this could change the magnetic response of the involved spins, which can be strongly pinned in canted directions.[47] A large local magneto-crystalline anisotropy almost randomly generated by the surface spin disorder prevents complete alignment of the magnetic moment inside the particle,[46,48] reducing the effective magnetic dipole. Furthermore, the interparticle interaction due to the surface charges of nanoparticles may increase the energy barrier for the magnetization reversal.[49,50] However, at higher magnetic field, the influence of magnetic interactions between the nanoparticles becomes less significant.[51] Thus, the effect of interparticle interaction on the reduction of saturation magnetization is weak.

For aminosilane and carboxyl-coated samples, the coatings are linked to the surface of magnetic core through hydrolysis reaction and the formation of Si−O and C−O bonds.[52] The

dx.doi.org/10.1021/la3022479 | Langmuir 2012, 28, 13051−13059

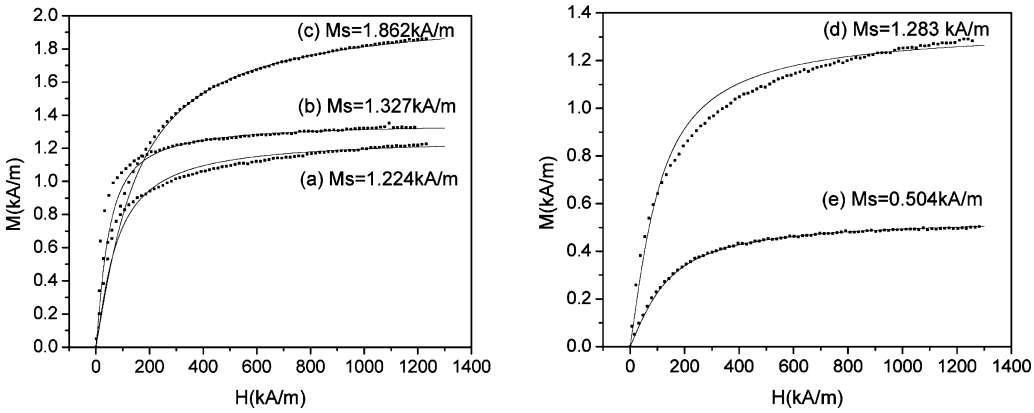

Figure 6. Experimental (■) and predicted (−) magnetization as a function of the applied field for (a) FluidMAG-UC/A, (b) FluidMAG-Amine, (c) FluidMAG-CMX, (d) MAG/OA-HEP, and (e) MAG/OA-HEX.

maximum reduction of magnetic phase is observed in FluidMAG-Amine sample, where the average thickness of the nonmagnetic phase is approximately 1.5 nm, while the minimum reduction of magnetic phase occurs in FluidMAG-CMX, which is 0.54 nm (Table 2). It has been reported that the saturation magnetization of ferrite nanoparticles decreases with decreasing particle size,[53] although the nature of this effect remains unclear.[54] Most studies attribute it to the adsorption of the surfactant molecules onto the particle surface,[18−20] which causes the spins of the iron atoms close to the surface to be pinned.[55] The coatings also influence the canting angles of magnetic moments of Fe atoms in its magnetic sublattice, producing magnetic disorder to a different extent.[56] Different coatings exhibiting different interactions with the magnetic core are expected to produce varying effects, leading to unique effective nonmagnetic layer thicknesses.

For oleic acid-coated nanoparticle samples, the adsorption of surfactant molecules onto the particle surface through COO− group bonding with Fe also leads to the formation of magnetically disordered layer. The reduction percentages of the magnetic phase depends on the solvent used to suspend the particles as previously shown in the literature,[18] which reported that magnetite nanoparticles of ∼5 nm in diameter coated with oleic acid experienced a magnetic phase reduction of 0.4 in kerosene and 0.47 in fluorocarbon. In this work, the observed reduction is 0.53 in heptane and 0.6 in hexane. The corresponding thickness of the nonmagnetic layer is 0.58 and 0.97 nm, respectively. The lower thickness of nonmagnetic layer of nanoparticles in heptane may be attributed to higher adsorption of oleic acid in heptanes; heptane has a higher limiting adsorption value (2.4 mmol/g) than hexane (1.6 mmol/g) for oleic acid-coated magnetic nanoparticles.[57,58] Thus, it is possible that heptane hinders the interactions between oleic acid and magnetite core to a greater extent and, therefore, causes thinner nonmagnetic layer formation.

4. CONCLUSION

In the current work, magnetization measurements and Tiron chelation test were used to determine the mass concentration of magnetic core and original magnetite in ferrofluids. Magnetic nanoparticles with different biocompatible coatings or uncoated in the same solvent (water), in parallel with oleic acid covered particles suspended in hexane and heptane, were studied. It was found that the reduction of magnetic phase in nanoparticles varies with different coatings as well as solvents. The magnetic phase reduction observed in commercial samples may be due to the surface spin disorder influenced by the absorbance of coatings and electric charge. For oleic acid-coated samples, the difference observed in the magnetic phase reduction may be attributed to the effect of the solvents, which may change the strength of the interaction of the coating and the magnetic core.

In conclusion, to optimize the properties of magnetic nanoparticles for biomedical applications, it is essential to consider the reduction of magnetic phase in the presence of various biocompatible coating or suspension media. This interaction affects not only the effective magnetic phase concentration, but also other phenomena depending on the size of the magnetic core such as relaxation.

■ ASSOCIATED CONTENT

Ⓢ Supporting Information

Additional experimental information. This material is available free of charge via the Internet at http://pubs.acs.org.

■ AUTHOR INFORMATION

Corresponding Author

*E-mail: borcad@rpi.edu.

Notes

The authors declare no competing financial interest.

■ ACKNOWLEDGMENTS

D.-A.B.-T. acknowledges NSF award 0846433. R.O. acknowledges partial support from IBM. D.R. is supported by TUBITAK 2219 Program.

■ REFERENCES

(1) Mikhaylova, M.; Kim, D. K.; Bobrysheva, N.; Osmolowsky, M.; Semenov, V.; Tsakalakos, T.; Muhammed, M. Superparamagnetism of magnetite nanoparticles: Dependence on surface modification. *Langmuir* **2004**, *20*, 2472−2477.

(2) Talelli, M.; Rijcken, C. J. F.; Lammers, T.; Seevinck, P. R.; Storm, G.; van Nostrum, C. F.; Hennink, W. E. Superparamagnetic iron oxide nanoparticles encapsulated in biodegradable thermosensitive polymeric micelles: Toward a targeted nanomedicine suitable for image-guided drug delivery. *Langmuir* **2009**, *25*, 2060−2067.

(3) Mahmoudi, M.; Simchi, A.; Imani, M.; Häfeli, U. O. Superparamagnetic iron oxide nanoparticles with rigid cross-linked polyethylene glycol fumarate coating for application in imaging and drug delivery. *J. Phys. Chem. C* **2009**, *113*, 8124−8131.

(4) Quan, Q.; Xie, J.; Gao, H.; Yang, M.; Zhang, F.; Liu, G.; Lin, X.; Wang, A.; Eden, H. S.; Lee, S.; Zhang, G.; Chen, X. HSA coated iron

oxide nanoparticles as drug delivery vehicles for cancer therapy. *Mol. Pharmaceutics* **2011**, *8*, 1669−1676.
(5) Beveridge, J. S.; Stephens, J. R.; Williams, M. E. The use of magnetic nanoparticles in analytical chemistry. *Annu. Rev. Anal. Chem.* **2011**, *4*, 251−273.
(6) Smith, J. E.; Sapsford, K. E.; Tan, W.; Ligler, F. S. Optimization of antibody-conjugated magnetic nanoparticles for target preconcentration and immunoassays. *Anal. Biochem.* **2011**, *410*, 124−132.
(7) Aguilar-Arteaga, K.; Rodriguez, J. A.; Barrado, E. Magnetic solids in analytical chemistry: A review. *Anal. Chim. Acta* **2010**, *674*, 157−165.
(8) Santra, S.; Kaittanis, C.; Grimm, J.; Perez, J. M. Drug/dye-loaded, multifunctional iron oxide nanoparticles for combined targeted cancer therapy and dual optical/magnetic resonance imaging. *Small* **2009**, *5*, 1862−1868.
(9) Yang, X.; Hong, H.; Grailer, J. J.; Rowland, I. J.; Javadi, A.; Hurley, S. A.; Xiao, Y.; Yang, Y.; Zhang, Y.; Nickles, R. J.; Cai, W.; Steeber, D. A.; Gong, S. cRGD-functionalized, DOX-conjugated, and 64Cu-labeled superparamagnetic iron oxide nanoparticles for targeted anticancer drug delivery and PET/MR imaging. *Biomaterials* **2011**, *32*, 4151−4160.
(10) Daldrup-Link, H. E.; Golovko, D.; Ruffell, B.; DeNardo, D. G.; Castaneda, R.; Ansari, C.; Rao, J.; Tikhomirov, G. A.; Wendland, M. F.; Corot, C.; Coussens, L. M. MRI of tumor-associated macrophages with clinically applicable iron oxide nanoparticles. *Clin. Cancer Res.* **2011**, *17*, 5695−5704.
(11) Andreas, K.; Georgieva, R.; Ladwig, M.; Mueller, S.; Notter, M.; Sittinger, M.; Ringe, J. Highly efficient magnetic stem cell labeling with citrate-coated superparamagnetic iron oxide nanoparticles for MRI tracking. *Biomaterials* **2012**, *33*, 4515−4525.
(12) Hou, C.-H.; Hou, S.-M.; Hsueh, Y.-S.; Lin, J.; Wu, H.-C.; Lin, F.-H. The in vivo performance of biomagnetic hydroxyapatite nanoparticles in cancer hyperthermia therapy. *Biomaterials* **2009**, *30*, 3956−3960.
(13) Kievit, F. M.; Zhang, M. Surface engineering of iron oxide nanoparticles for targeted cancer therapy. *Acc. Chem. Res.* **2011**, *44*, 853−862.
(14) Day, E.; Morton, J.; West, J. Nanoparticles for thermal cancer therapy. *J. Biomech. Eng.* **2009**, *131*, 5.
(15) Grüttner, C.; Müller, K.; Teller, J.; Westphal, F.; Foreman, A.; Ivkov, R. Synthesis and antibody conjugation of magnetic nanoparticles with improved specific power absorption rates for alternating magnetic field cancer therapy. *J. Magn. Magn. Mater.* **2007**, *311*, 181−186.
(16) Rosensweig, R. E. Heating magnetic fluid with alternating magnetic field. *J. Magn. Magn. Mater.* **2002**, *252*, 370−374.
(17) Krishnan, K. Biomedical nanomagnetic: A spin through possibilities in imaging, diagnostics, and therapy. *IEEE Trans. Magn.* **2010**, *46*, 2523−2558.
(18) Kaiser, R.; Miskolczy, G. Magnetic properties of stable dispersions of subdomain magnetite particles. *J. Appl. Phys.* **1970**, *41*, 1064−1072.
(19) Chantrell, R.; Pollplewell, J.; Charles, S. Measurements of particle size distribution parameters in ferrofluids. *IEEE Trans. Magn.* **1978**, *14*, 975−977.
(20) Vestal, C. R.; Zhang, Z. J. Effects of surface coordination chemistry on the magnetic properties of MnFe2O4 spinel ferrite nanoparticles. *J. Am. Chem. Soc.* **2003**, *125*, 9828−9833.
(21) Chemicell Magnetic Nanoparticles; http://www.chemicell.com.
(22) Kohler, N.; Fryxell, G. E.; Zhang, M. A bifunctional poly(ethylene glycol) silane immobilized on metallic oxide-based nanoparticles for conjugation with cell targeting agents. *J. Am. Chem. Soc.* **2004**, *126*, 7206−7211.
(23) McCarthy, J. R.; Weissleder, R. Multifunctional magnetic nanoparticles for targeted imaging and therapy. *Adv. Drug Delivery Rev.* **2008**, *60*, 1241−1251.
(24) Sun, S.; Zeng, H.; Robinson, D. B.; Raoux, S.; Rice, P. M.; Wang, S. X.; Li, G. Monodisperse MFe_2O_4 (M = Fe, Co, Mn) nanoparticles. *J. Am. Chem. Soc.* **2003**, *126*, 273−279.
(25) Kataby, G.; Cojocaru, M.; Prozorov, R.; Gedanken, A. Coating carboxylic acids on amorphous iron nanoparticles. *Langmuir* **1999**, *15*, 1703−1708.
(26) Yoe, J.; Jones, A. Colorimetric determination of iron with disodium 1,2-dihydroxybenzene-3,5-disulfonate. *Ind. Eng. Chem.* **1944**, *16*, 111−115.
(27) Accelrys Software Inc. Materials Studio; http://accelrys.com.
(28) Slavov, L.; Abrashev, M. V.; Merodiiska, T.; Gelev, C.; Vandenberghe, R. E.; Markova-Deneva, I.; Nedkov, I. Raman spectroscopy investigation of magnetite nanoparticles in ferrofluids. *J. Magn. Magn. Mater.* **2010**, *322*, 1904−1911.
(29) de Faria, D.; Venancio Silva, S.; de Oliveira, M. Raman microspectroscopy of some iron oxides and oxyhydroxides. *J. Raman Spectrosc.* **1997**, *28*, 873−878.
(30) Hanesch, M. Raman spectroscopy of iron oxides and (oxy)hydroxides at low laser power and possible applications in environmental magnetic studies. *Geophys. J.* **2009**, *177*, 941−948.
(31) Shebanova, O. N.; Lazor, P. Raman spectroscopic study of magnetite ($FeFe_2O_4$): a new assignment for the vibrational spectrum. *J. Solid State Chem.* **2003**, *174*, 424−430.
(32) Chourpa, I.; Douziech-Eyrolles, L.; Ngaboni-Okassa, L.; Fouquenet, J.-F.; Cohen-Jonathan, S.; Souce, M.; Marchais, H.; Dubois, P. Molecular composition of iron oxide nanoparticles, precursors for magnetic drug targeting, as characterized by confocal Raman microspectroscopy. *Analyst* **2005**, *130*, 1395−1403.
(33) Pinna, N.; Grancharov, S.; Beato, P.; Bonville, P.; Antonietti, M.; Niederberger, M. Magnetite nanocrystals: Nonaqueous synthesis, characterization, and solubility. *Chem. Mater.* **2005**, *17*, 3044−3049.
(34) Legodi, M. A.; de Waal, D. The preparation of magnetite, goethite, hematite and maghemite of pigment quality from mill scale iron waste. *Dyes Pigm.* **2007**, *74*, 161−168.
(35) Soler, M. A. G.; Alcantara, G. B.; Soares, F. Q.; Viali, W. R.; Sartoratto, P. P. C.; Fernandez, J. R. L.; da Silva, S. W.; Garg, V. K.; Oliveira, A. C.; Morais, P. C. Study of molecular surface coating on the stability of maghemite nanoparticles. *Surf. Sci.* **2007**, *601*, 3921−3925.
(36) Tang, J.; Myers, M.; Bosnick, K. A.; Brus, L. E. Magnetite Fe_3O_4 nanocrystals: Spectroscopic observation of aqueous oxidation kinetics. *J. Phys. Chem. B* **2003**, *107*, 7501−7506.
(37) Daou, T. J.; Pourroy, G.; Bégin-Colin, S.; Grenèche, J. M.; Ulhaq-Bouillet, C.; Legaré, P.; Bernhardt, P.; Leuvrey, C.; Rogez, G. Hydrothermal synthesis of monodisperse magnetite nanoparticles. *Chem. Mater.* **2006**, *18*, 4399−4404.
(38) Xuan, S.; Hao, L.; Jiang, W.; Gong, X.; Hu, Y.; Chen, Z. Preparation of water-soluble magnetite nanocrystals through hydrothermal approach. *J. Magn. Magn. Mater.* **2007**, *308*, 210−213.
(39) Aronniemi, M.; Lahtinen, J.; Hautojärvi, P. Characterization of iron oxide thin films. *Surf. Interface Anal.* **2004**, *36*, 1004−1006.
(40) Moulder, J.; Stickle, W.; Sobol, P.; Bomben, K. *Handbook of X-ray Photoelectron Spectroscopy*; ULVAC-PHI Inc.: Chigasaki, Japan, 1995.
(41) Monti, M.; Santos, B.; Mascaraque, A.; Rodríguez de la Fuente, O.; Niño, M. A.; Menteş, T. O.; Locatelli, A.; McCarty, K. F.; Marco, J. F.; de la Figuera, J. Magnetism in nanometer-thick magnetite. *Phys. Rev. B* **2012**, *85*, 020404.
(42) Iconaru, S.; Andronescu, E.; Ciobanu, C.; Prodan, A.; Le Coustumer, P.; Predoi, D. Biocompatible magnetic iron oxide nanoparticles doped dextran thin films produced by spin coating deposition solution. *Digest J. Nanomater. Biostruct.* **2012**, *7*, 399−409.
(43) Sugimura, H.; Hozumi, A.; Kameyama, T.; Takai, O. Organosilane self-assembled monolayers formed at the vapour/solid interface. *Surf. Interface Anal.* **2002**, *34*, 550−554.
(44) Bratt, A.; Barron, A. XPS of Carbon Nanomaterials; http://cnx.org/content/m34549/1.2/.
(45) Yuan, Y.; Borca-Tasciuc, D. A. Comparison between experimental and predicted specific absorption rate of functionalized iron oxide nanoparticle suspensions. *J. Magn. Magn. Mater.* **2011**, *323*, 2463−2469.

(46) Kihal, A.; Fillion, G.; Bouzabata, B.; Barbara, B. High field surface magnetic study of Fe_3O_4 nanoparticles. *Phys. Status Solidi B* **2012**, *249*, 604−614.
(47) Rebodos, R. L.; Vikesland, P. J. Effects of oxidation on the magnetization of nanoparticulate magnetite. *Langmuir* **2010**, *26*, 16745−16753.
(48) Ozkaya, T.; Toprak, M. S.; Baykal, A.; Kavas, H.; Köseoğlu, Y.; Aktaş, B. Synthesis of Fe_3O_4 nanoparticles at 100 °C and its magnetic characterization. *J. Alloys Compd.* **2009**, *472*, 18−23.
(49) Dormann, J. L.; Spinu, L.; Tronc, E.; Jolivet, J. P.; Lucari, F.; D'Orazio, F.; Fiorani, D. Effect of interparticle interactions on the dynamical properties of γ-Fe_2O_3 nanoparticles. *J. Magn. Magn. Mater.* **1998**, *183*, L255−L260.
(50) Vestal, C. R.; Song, Q.; Zhang, Z. J. Effects of interparticle interactions upon the magnetic properties of $CoFe_2O_4$ and $MnFe_2O_4$ nanocrystals. *J. Phys. Chem. B* **2004**, *108*, 18222−18227.
(51) Fonnum, G.; Johansson, C.; Molteberg, A.; Mørup, S.; Aksnes, E. Characterisation of Dynabeads by magnetization measurements and Mössbauer spectroscopy. *J. Magn. Magn. Mater.* **2005**, *293*, 41−47.
(52) Herrera, A. P.; Barrera, C.; Rinaldi, C. Synthesis and functionalization of magnetite nanoparticles with aminopropylsilane and carboxymethyldextran. *J. Mater. Chem.* **2008**, *18*, 3650−3654.
(53) Morales, M. P.; Veintemillas-Verdaguer, S.; Montero, M. I.; Serna, C. J.; Roig, A.; Casas, L.; Martínez, B.; Sandiumenge, F. Surface and internal spin canting in γ-Fe2O3 nanoparticles. *Chem. Mater.* **1999**, *11*, 3058−3064.
(54) Yamaura, M.; Camilo, R. L.; Sampaio, L. C.; Macêdo, M. A.; Nakamura, M.; Toma, H. E. Preparation and characterization of (3-aminopropyl)triethoxysilane-coated magnetite nanoparticles. *J. Magn. Magn. Mater.* **2004**, *279*, 210−217.
(55) Blanco-Mantecón, M.; O'Grady, K. Interaction and size effects in magnetic nanoparticles. *J. Magn. Magn. Mater.* **2006**, *296*, 124−133.
(56) Roca, A. G.; Niznansky, D.; Poltierova-Vejpravova, J.; Bittova, B.; Gonzalez-Fernandez, M. A.; Serna, C. J.; Morales, M. P. Magnetite nanoparticles with no surface spin canting. *J. Appl. Phys.* **2009**, *105*, 114309−7.
(57) Korolev, V.; Ramazanova, A.; Yashkova, V.; Balmasova, O.; Blinov, A. Adsorption of fatty acids from solutions in organic solvents on the surface of finely dispersed magnetite: 1. Isotherms of adsorption of oleic, linoleic, and linolenic acid from carbon tetrachloride and hexane. *Colloid J.* **2004**, *66*, 700−704.
(58) Korolev, V.; Balmasova, O.; Ramazanova, A. The sorption isotherms of oleic, linoleic, and linolenic acids from solutions in cyclohexane and heptane on magnetite. *Russ. J. Phys. Chem. A* **2009**, *83*, 1018−1021.